Materialia 24 (2022) 101487

Contents lists available at ScienceDirect

Materialia

journal homepage: www.elsevier.com/locate/mtla

Understanding the mechanism of shockwave induced graphite-to-diamond phase transition

Haofan Sun[a], Xinyu Jiang[a], Rui Dai[a], Lei Liu[a], Zuyuan Wang[b], Xing Zhang[c], Houlong Zhuang[a,*], Yiliang Liao[c,*], Qiong Nian[a,*]

[a] School of Engineering for Matter, Transport and Energy, Arizona State University, Tempe, AZ 85287, USA
[b] School of Mechanical and Electrical Engineering, University of Electronic Science and Technology of China, Chengdu, Sichuan 611731, China
[c] Department of Industrial & Manufacturing Systems Engineering, Iowa State University, Ames, IA 50011, USA

ARTICLE INFO

Keywords:
Graphite-to-diamond transition
Shockwave synthesis
Molecular dynamics

ABSTRACT

Nanodiamonds (NDs) manufactured from graphite exhibit superior physical properties that are desired in enormous applications, but the graphite-to-diamond phase transition mechanism in nonequilibrium synthesis is poorly understood, hindering the optimization and control of the manufacturing process. Herein, in this paper, molecular dynamics and density function theory simulations were conducted to unravel the graphite-to-diamond phase transition mechanism in the shockwave-based ND manufacturing process. Our simulations first reveal the synergistic effect of incident and reflected shockwaves, which stabilizes the positions of carbon atoms, leading to the formation of the interlayer carbon bonds and diamond phase. Moreover, simulation results exhibit the tiered movement of the graphite layers and the frequent exchange of kinetic energy between the adjacent graphite layers, indicating the propagation of the incident shockwaves and the initiation of the reflected shockwaves. Finally, the simulations shed light on the origin of the byproduct such as amorphous carbon and carbon liquid during the shockwave-based ND manufacturing. This work advances the fundamental understanding of the graphite-to-diamond phase transition mechanism and will promote the design and optimization of related manufacturing processes.

1. Introduction

Diamond nanoparticles, namely nanodiamonds (NDs), containing two sp^3 carbon atoms in its primitive (Bravais) cell, commonly belong to the face-centered cubic (FCC) crystal system [1]. Its distinct crystal structure brings exceptional physical properties, such as high hardness, low thermal expansion coefficient, and high thermal conductivity, leading to its widespread applications [2]. For instance, as one of the hardest materials, NDs have been extensively utilized as a wear-resistant coating for cutting and grinding tools [1–3]. Its advantages of electrical insulation, broad optical transparency and doping capability allow NDs to be widely accepted as insulators and optical components. In addition, NDs' truncated octahedral morphology, rich surface chemistry and excellent biocompatibility allow them to be utilized as bioimaging agents and drug carriers [1,2,4–8].

Despite their promising properties and broader impacts in applications, nanomanufacturing of NDs remains challenging. A variety of nanomanufacturing technologies (equilibrium or nonequilibrium synthesis), have been developed for ND fabrication. The equilibrium high temperature high pressure (HTHP) synthesis often requires a metal-carbon catalytic system, bulky anvils, and a relatively long reaction time [9,10]. Other equilibrium synthesis method, such as chemical vapor deposition (CVD), can grow high quality diamond phase from gaseous resources, but it typically requires high vacuum chamber, precise control of gas, complex pretreatment, and diamond crystals as seeds [5,11–13]. On the other hand, a number of studies have been conducted to develop non-equilibrium processes for ND synthesis directly from graphite. One widely known non-equilibrium ND fabrication process is shockwave synthesis (as illustrated in Fig. 1a), where the shockwaves are utilized to promote the graphite-to-diamond phase transition [7,14–19]. The shockwave generates a localized HTHP environment in a short duration to overcome the extra-high activation energy for the graphite-to-diamond phase transition [7,15–19]. In addition to the phase diagram shown in Fig. 1a, some previous studies indicate a diamond instability zone between 55 GPa and 115 GPa, which requires further study to confirm. However, this is not in the scope of this study [20,21].

A few nanomanufacturing strategies were developed for generating the shockwaves towards ND fabrication, such as chemical detonation, ultrasonic cavitation, pulsed laser ablation and among many others [22,23]. NDs were first synthesized in 1960s by Soviet scientists us-

* Corresponding authors.
E-mail addresses: hzhuang7@asu.edu (H. Zhuang), leonl@iastate.edu (Y. Liao), qiong.nian@asu.edu (Q. Nian).

https://doi.org/10.1016/j.mtla.2022.101487
Received 5 May 2022; Accepted 20 June 2022
Available online 21 June 2022

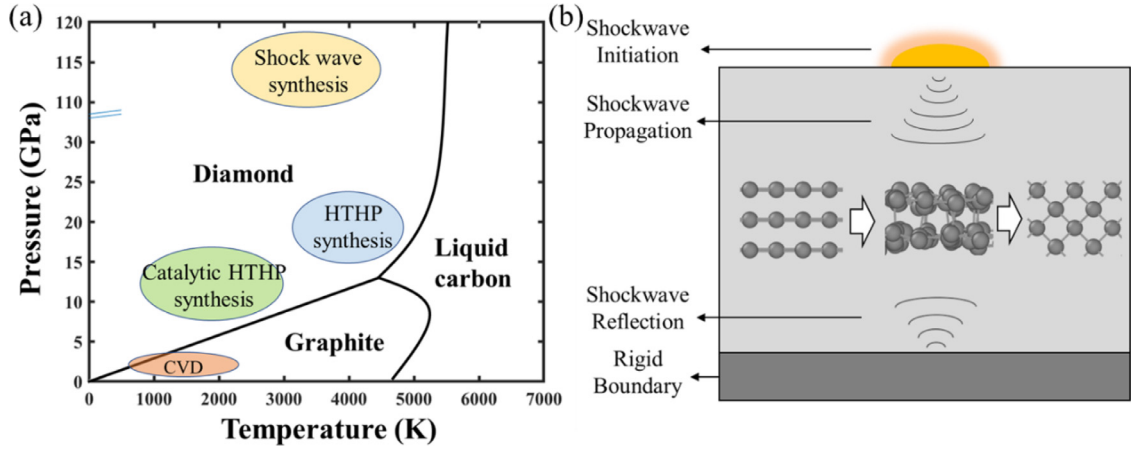

Fig. 1. (a) Nanomanufacturing strategies for ND fabrication [27,28]. (b) Schematic illustration of the graphite-to-diamond transition induced by shockwave propagation and reflection.

ing a detonation method [24]. In these processes, the characteristics of explosion-induced shockwaves, particularly the shock velocity or duration, play key roles on determining the graphite-to-diamond transition phenomena, as illustrated in Fig. 1b. However, previous experimental observations demonstrated that the yield of diamond phase in the shockwave synthesis process is low and related to the propagation direction of shockwaves. For example, Khachatryan. et al. showed that there is a high probability to activate the graphite-to-diamond phase transition only when the ultrasonic cavitation collapse is normal to the graphite crystal lattices [25]. Despite these advancements, the mechanism responsible for the shockwave-induced graphite-to-diamond transition is still vague, especially at the atomic level. Specific scientific questions to answer include: (i) how the propagation and reflection of shockwaves in the graphite lattice contribute to the diamond phase initiation; (ii) how do the shock velocity and shock duration affect the yield rate of diamond crystals [26]; and (iii) what are the potential byproducts of these processes. Although these questions cannot be easily addressed by experiments due to the experimental difficulties particularly at the atomic level, computational simulation provides a robust tool to pave the way towards elucidation of the fundamental process mechanism involved in the shockwave-induced ND fabrication.

In this work, molecular dynamics (MD) simulations were performed to study the graphite-to-diamond phase transition mechanism in the shockwave-based ND manufacturing process. It is found the velocity and duration of incident shockwaves as well as synergistic reflected shockwaves significantly affect the formation of the interlayer carbon bonds and diamond phase. Then, ab-initio molecular dynamics (AIMD) were performed to further study the shock induced diamond phase formation without using empirical potentials, reconfirming the simulation results, and decreasing the computational costs. Thus, through MD and AIMD simulations, we could investigate the role of shockwaves in graphite-to-diamond conversion at atomic level. In this study, we mainly discuss the behavior of shockwaves and their influences on diamond formation based on MD and AIMD simulations.

2. Computational modeling

2.1. MD simulations

To simulate the shockwave propagation in the graphite lattice, we created a three-dimensional (3D) computational cell (Fig. 2a and 2e) with the initial supercell size of $V_0 = 2.40 \times 2.12 \times 14.92$ nm^3 and 9000 carbon atoms in total (45 layers and 200 carbon atoms per layer). These carbon atoms were assigned with initial velocities according to a Gaussian distribution at $T = 300$ K, and then thermally equilibrated in the isothermal–isobaric (NPT) ensemble at a pressure of 0 MPa for 1 ns and in the microcanonical (NVE) ensemble for 1 ns. The timestep used for the thermal equilibration was 1 fs. We set periodic boundary conditions along all axes during equilibration, leading to a nominal bulk density of graphite $\rho_0 = 2.343$ g/cm^3 (cell volume $2.42 \times 2.10 \times 15.06$ nm^3). For the shock simulation, the periodic boundary conditions along the z axis were removed. The shock was generated by a rigid piston constituted by fixed atoms of one layer of graphene and moved at a constant velocity u_p along the z axis. At the opposite side of the piston, two layers of carbon atoms were fixed to generate the reflected shockwaves. Shock simulations were conducted in the NVE ensemble with a timestep of 0.1 fs and for a time sufficiently long to ensure the reflected shockwave to return and affect the atomic structure. To observe the interlayer bonds, we set the cutoff distance at 1.6 Å, which was close to the representative bond length of sp3-sp3 carbon atoms (1.54 Å). The simulations were performed using the LAMMPS package and the potential file AIREBO-M [29,30]. The results were analyzed by Ovito and Python [31].

2.2. AIMD simulations

Based on the results of MD simulation, AIMD was applied to investigate the carbon phase transitions under different shockwave-compression timesteps. Excluding the first layer of carbon atoms in MD simulation (the first layer was fixed as piston), the second to fifth layers were chosen for the AIMD model with 100 atoms/layer. Considering the inconsistent change of compression rate $\Delta V/V_0$, four initial graphite structures were selected from different simulation timesteps (0, 1.2, 2.4 and 3.6 ps), during which the position of these carbon atoms were extracted and replicated in the AIMD model. The NVE ensemble was applied in these four structures with a timestep of 0.1 fs. The Vienna *Ab initio* Simulation Package (VASP) was applied with the generalized gradient approximation (GGA) parameterized by Perdew, Burke, and Ernzerhof (PBE) [32] for the exchange-correlation functional and the cutoff energy of 400 eV for the plane wave basis [33,34]. The *k* points were set to 1 because of the model size (12 Å × 21 Å × 13 Å at 0 ps). To be consistent with the MD simulations, the temperatures of the initial four graphite structures were extracted from MD model at 0, 1.2, 2.4 and 3.6 ps, respectively, and input into the AIMD models. The results were analyzed by Ovito [31].

3. Results and discussion

3.1. MD simulation of shockwave on graphite

According to prior reports, graphite-to-diamond phase transition can happen under a broad range of shock conditions, e.g., shockwave veloc-

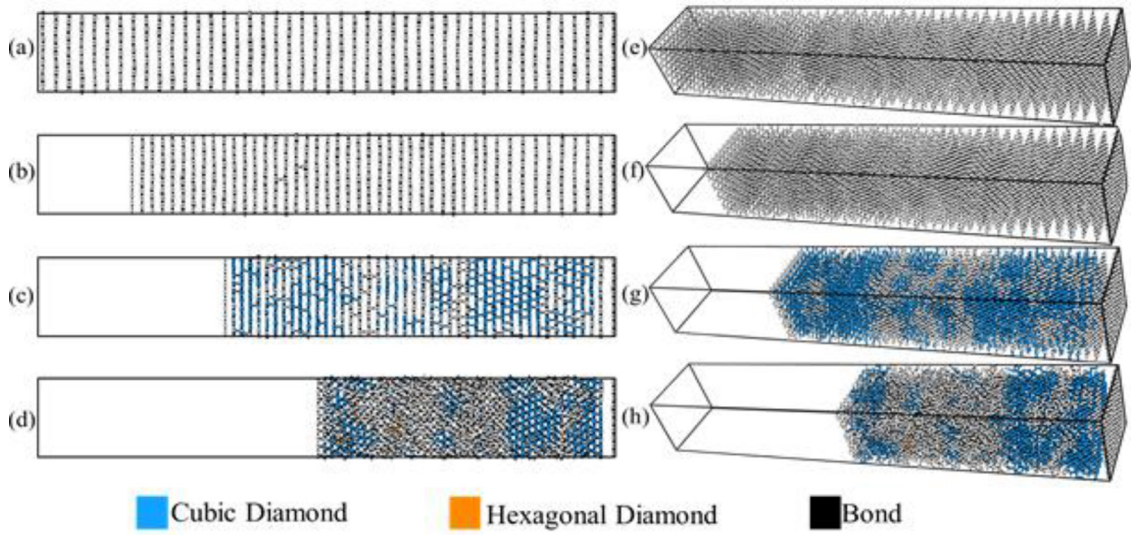

Fig. 2. Different timesteps of the front view and the perspective view of graphite model under 2 km/s piston velocity. (a, e)0.0 ps. (b, f)1.2 ps. (c, g)2.4 ps. (d, h)3.6 ps. (Unidentified atoms are colored in white.).

ity up to 20 km/s corresponding to 8 km/s for piston velocity in the MD model [35–38]. As seen below, the shockwave velocity is correlated with the piston velocity in the linear approximation of the velocity Hugoniot relationship:

$$U_s = sU_p + c_0 \tag{1}$$

Where U_S is the velocity of an incident wave, U_P is the velocity of piston, s is a parameter, $c_0 = \sqrt{c_{11}/\rho_0}$ is the sound speed in the undeformed mono-dimensional elastic medium (c_{11} is the Young's modulus perpendicular to graphite planes).

Herein, to study the shockwave propagation in graphite lattice and its impacts on potential phase change, we started the simulation by selecting a piston velocity of 1 km/s and then increased it up to 8 km/s. Fig. 2 depicts the atoms reconfiguration and layers restructuring in the graphite model during the 2 km/s piston shock process. As shown, the layered structure of graphite is preserved in the whole sample before shock starts (Fig. 2a). Along with the propagation of shockwave towards graphite, the interlayer spacing decreases following by the formation of few interlayer bonds as presented in Fig. 2b. In Fig. 2c, it is observed that an increasing number of interlayer bonds and the cubic and hexagonal diamond structures are formed at the simulation time of 2.4 ps, which implies the sp2 to sp3 transformation of carbon atoms. Further propagation of shockwaves in Fig. 2d at a simulation time of 3.6 ps however results in a large amount of disordered and unbonded carbon atoms, which were considered as amorphous carbon byproduct in previous studies [4,6]. Though the layered graphite structure collapses, it can be seen that a certain amount of diamond structures still exist. A clear visualization of the graphite structure evolution during the shockwave propagation can be observed in the 3D models in Fig. 2e–h as well.

Noteworthy, to identify whether the carbon atoms are graphite or diamond phase in our MD model, the diamond analysis function of Ovito is operated, applying the Common Neighbor Analysis method (CNA) [39]. Instead of considering the 1st neighbors of central carbon atoms, CNA method computes the distance between central atoms to its 2nd neighbors. When the 2nd neighbors apply to a cubic diamond or hexagonal diamond structure, the central, 1st and 2nd neighbor carbon atoms are identified. This method has been used extensively in previous studies [38]. However, it overestimates the graphite-to-diamond transition rate reckoning without 1st neighbor atoms. By considering the interlayer bonds, we took 1st neighbors into account to solve this problem. Thus, only with an interlayer bond, the identified atom would be considered as a cubic or hexagonal diamond atom in this study.

Not only the shockwave propagation but also the shockwave velocity will have significant impacts on the graphite-to-diamond phase transition. To study the influence of the shockwave velocities, a series of models were run in Fig. 3. In these models, different piston velocities at the same compression rate $\Delta V/V_0 = 0.35$ were implemented, while this volume compression rate is selected based on the shockwave propagation analysis discussed above. Fig. 3a–c show interlayer spacing almost equally decreases after shock compression under piston velocities from 1 to 4 km/s, while Fig. 3d, e shows a more compacted structure on the left side compared with the right side of the model under piston velocities from 6 to 8 km/s. This can be explained that for piston velocity u_p <= 4 km/s, the shockwave propagates slowly, which would allow the top layers on the left side to transfer the shock compression to the bottom layers on the right side. Therefore, each layer of graphite lattice is almost uniformly compressed leading to the almost equal decrease of interlayer spacing. The reason we use "almost" here, is because the shockwave compression is a dynamic process, during which the carbon atoms and graphite layers are always moving, thereby the interlayer spacing would not be perfectly equal.

Universally and relative uniformly decreased interlayer spacing would facilitate the formation of interlayer bonds and diamond phases throughout the graphite lattice when there is sufficient kinetic energy input into the carbon atoms. Further investigating Fig. 3a–c, it is found faster piston velocities of 2 km/s and 4 km/s could generate faster shockwaves, thus provides higher kinetic energies to the carbon atoms. As a result, the carbon atoms are incited to vibrate abruptly and thereby overcome the rigorous lattice structure of graphite, and finally achieve the formation of interlayer bonds and diamond phases. On the contrary, in the model with 1 km/s piston velocity, very few interlayer bonds or diamond phases are observed due to insufficient kinetic energy input. For high piston velocities u_p>= 6 km/s in Fig. 3d, e, top layers tend to absorb the shock compression instead of transferring it to the bottom layers. In this respect, strong collisions happen between piston and top layers, leading to the formation of amorphous carbon and carbon liquid near the piston area. In addition, the diamond phases are only observed in the squeezed top layers of the graphite model, and the quantity of the formed diamond phase decreases along with increasing piston velocity. This implies one may not be able to obtain high graphite-to-diamond phase transition rate if an excessively intense shockwave is applied. To further study the internal structures of formed diamond phases, we sliced the model from 10~15 Å (Fig. 3f–j). Combining the top view images and the sliced view ones, it is clear to conclude that diamond phases

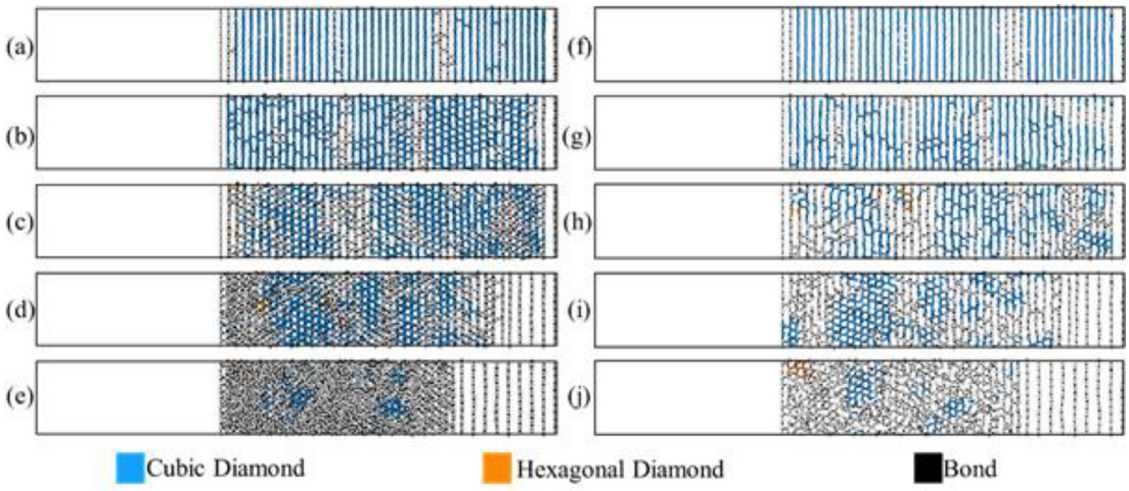

Fig. 3. Graphene model (a-e) and its slice(f-j) from 10 ~ 15 Å on x axis under different piston velocities (a, f)1 km/s. (b, g)2 km/s. (c, h)4 km/s. (d, i)6 km/s. (e, j)8 km/s at $\Delta V/V_0 = 0.35$. (Unidentified atoms are colored in white.).

formed during the shockwave compression are three-dimensional crystals. Fig. 3i, j show some diamond crystals still exist under high velocity piston compression, indicating the distinct mechanical properties of the diamond.

When studying the effect of piston velocities (U_P) on the phase transition in Fig. 3, intuitively, we think reflected shockwaves will be generated if the shock compression can be transferred to the bottom rigid "boundary" in low piston velocity models. The reflected shockwaves could bring about reverse momentum to the carbon atoms and graphite layers, interfering with incident shockwaves and thereby affecting the bonds formation and phase change. The large amount of interlayer bonds formed surrounding the bottom layer in Fig. 3b and 3c supports this hypothesis. In addition, the models with piston velocity of 2 km/s and 4 km/s in Fig. 3b and 3c could acquire the reflected shockwaves earlier than the one with a piston velocity of 1 km/s in Fig. 3a, due to faster incident shockwaves. This might be another reason why different numbers of interlayer bonds are observed in Fig. 3a–c. The synergistic effect of incident and reflected shockwaves deserves further study by tracing the movement of carbon atoms in the graphite models in following discussion.

To explore the synergistic effect of incident and reflected shockwaves on the diamond formation, we analyzed the reflected shockwaves under different piston velocities. We compared the counts of atom velocity on the z axis under piston velocities from 1 km/s to 8 km/s during the shock process (Fig. 4a). Vz>=0 means the atom moves towards the piston instead of the bottom of the graphite lattice, and vice versa. Due to the heat balance, the initial state is at around 4500 atoms. We observed the crests and troughs of the shockwaves in Fig. 4a. The troughs could be interpreted as the moment when incident shockwaves dominate; most of the atoms move towards the bottom of the model. While the crests could be interpreted as the moment when reflected shockwaves balance with the incident shockwaves, a relatively small number of atoms still move towards the bottom in the same direction as the piston, whereas a lot of them stop or reversely move toward the piston. These atom momentum changes render opportunities for interlayer carbon atoms to get close to each other for a prolong time period, thus benefiting the interlayer bonds formation, e.g., in lower piston velocities of 2 km/s and 4 km/s. In high piston velocities of 6 km/s and 8 km/s, the incident wave travels too fast to allow the reflected wave interaction. As seen in Fig. 4a, only one trend of reflected shockwaves is initiated at simulation time of 1000–1500 fs, which already induces intensive collision with incident shockwaves as seen in Fig. 3. Experimentally, this may explain why a large amount of amorphous carbon was formed in prior studies [3], agreeing well with the shock induced amorphization in brittle materials.

Besides, in very low piston velocity of 1 km/s, the incident wave travels very slow allowing long enough time to interact with the reflected shockwaves as shown in Fig. 4a with a series of crests and troughs, which thereby leading to interlayer spacing uniformly decreased. And until the simulation stops, the decreased interlayer spacing remains longer than the critical distance, thus extremely few interlayer bonds are formed. It is expected with further running the simulation, that is extending the shock duration time in practical experiments, diamond phase will be formed in the model later with least amorphous carbon byproducts. This also well explains previous experimental study [25], in which ultrasonic cavitation synthesized diamond particles demonstrated a much larger size than the laser shock synthesized ones, and we attribute the reason to much lower shockwave velocity with longer shockwave duration in the ultrasonic process.

To further review the effect of reflected shockwaves on diamond formation, the unidentified carbon atoms are removed to get a clear view in Fig. 4b (2 km/s piston velocity model). As seen in Fig. 4b, the diamond phase appears surrounding the bottom rigid boundary of the model at 1.6 ps, followed by a continuous growth from the bottom to top layers until 2.4 ps. The growth direction of diamond phase is in the same direction to the reflected shockwaves, confirming the fact that the reflected shockwaves stimulate the formation of diamonds. Besides, the gravity center on Z axis of diamond phase keeps moving up from 1.6 ps to 2.4 ps. The model also predicts the following decline of the gravity center on Z axis of the diamond phase in Fig. 4b insets from 2.4 ps to 3.2 ps and 3.9 ps, which is caused by the amorphization of the diamond phase in the over-compressed model. During this period, the carbon atoms could absorb more energy to break the sp3-sp3 carbon bonds, thereby become free to move, causing the collapse of diamond structures. We also can observe that the diamond phase in the upper layers almost diminish at 3.9 ps, which supports our idea that the further compression destructed the diamond phase in the model.

In summary of this analysis, it is concluded that the generation of the reflected shockwaves is significantly affected by the piston velocity or the "shock/detonation intensity" of the process, which further combines with shockwave duration time to determine the interlayer bonds formation and graphite-to-diamond phase transition. Thus, in the next section, we would like to further study the shockwave propagation and understand how the reflected wave is initiated using the 2 km/s model.

To analyze the propagation of shockwaves, we counted a set of parameters of 5th layer, 15th layer, 25th layer and 35th layer of the model

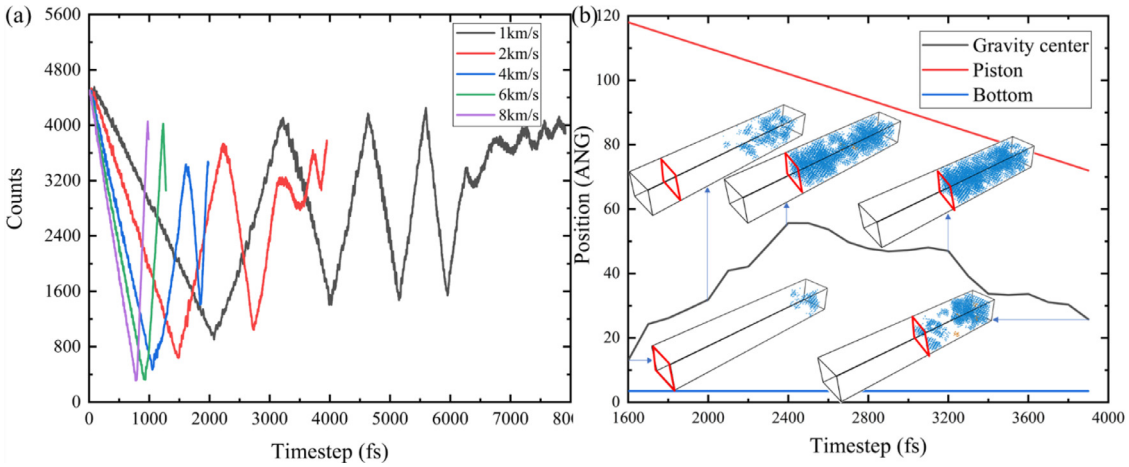

Fig. 4. (a) Counts for Vz>=0 under different piston velocities including 1 km/s, 2 km/s, 4 km/s, 6 km/s, 8 km/s. (b) The evolution of the gravity center of the diamond phase on Z axis in the model with 2 km/s piston velocity from 1.6 ps to 3.9 ps, the position of the piston (also annotated by red rhombus) and bottom of the model are also annotated as the reference objects (The cubic and hexagonal diamond carbon atoms are colored in blue and orange, respectively).

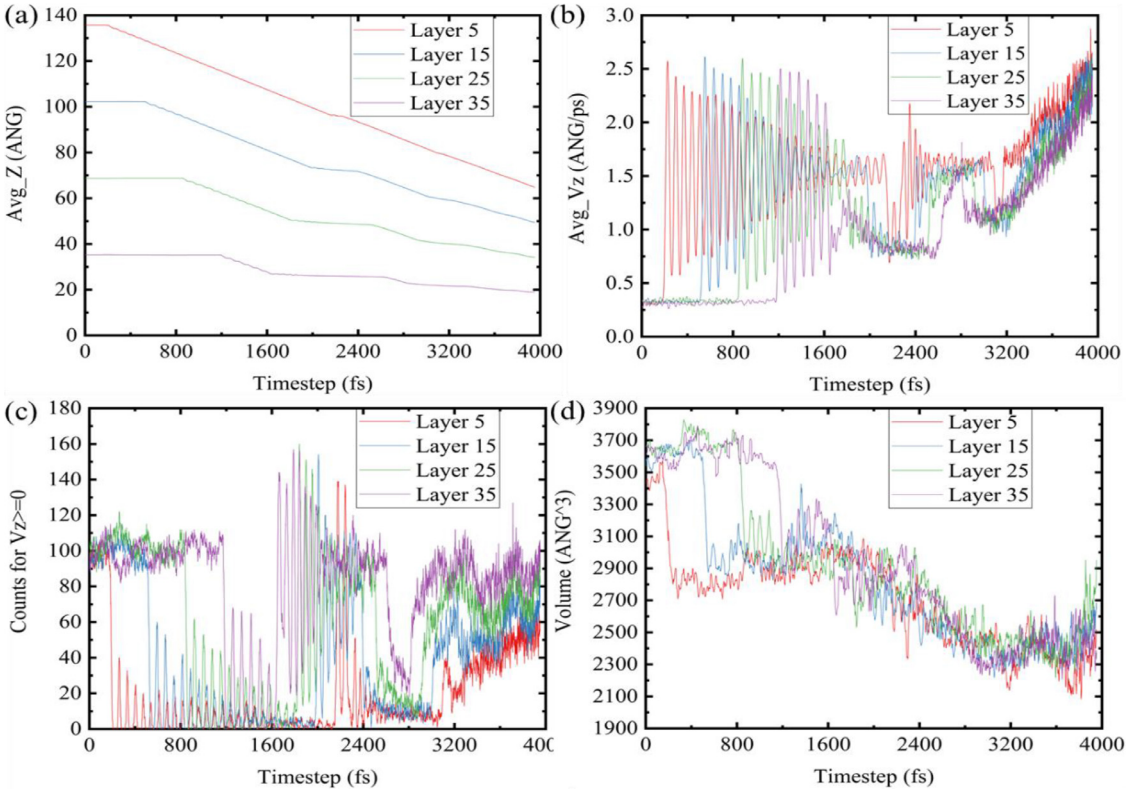

Fig. 5. Parameters during the simulation of laser shock on graphene layer 5, 15, 25, 35 at 2 km/s piston velocity. (a) average position at Z axis. (b) average velocity at the Z axis. (c) counts for Vz>=0. (d) volume around the layer.

(Fig. 5). By investigating the slope of the curve in Fig. 5a, we observed that the increasing slope occurs from 5th layer to 35th layer following the same moving direction of the piston, indicating the propagation of incident shockwaves. The decreasing slope occurs from the 35th layer to the 5th layer following the opposite moving direction of the piston, indicating the propagation of reflected shockwaves. Besides, we also observed two balancing stages in these curves. The duration of 1st balancing is ~100fs for the 5th layer, while it is ~1000fs for the 35th layer. Longer duration of balancing in the 35th layer implies the reflected shockwaves are stronger at the lower layers than the higher ones.

Fig. 5b reports the change of kinetic energy for atoms in each layer. We applied average velocity at Z axis to represent the kinetic energy of each layer, which is defined by:

$$Avg\_Vz = \frac{1}{n}\sum_{i=1}^{n}\sqrt{Vz_i{}^2} \tag{2}$$

Where i is the atom id, n is the number of atoms in each layer (in our model, n = 200), Vz_i is the velocity at Z axis for each atom, Avg_Vz is the average velocity at the Z axis of each graphite layer. The average velocity at the Z axis of each layer further confirms that the gains of kinetic energy occur from 5th layer to 35th layer following the same moving direction of the piston, indicating the propagation of incident shockwaves. While the losses of kinetic energy occur from the 35th layer to 5th layer following the opposite mov-

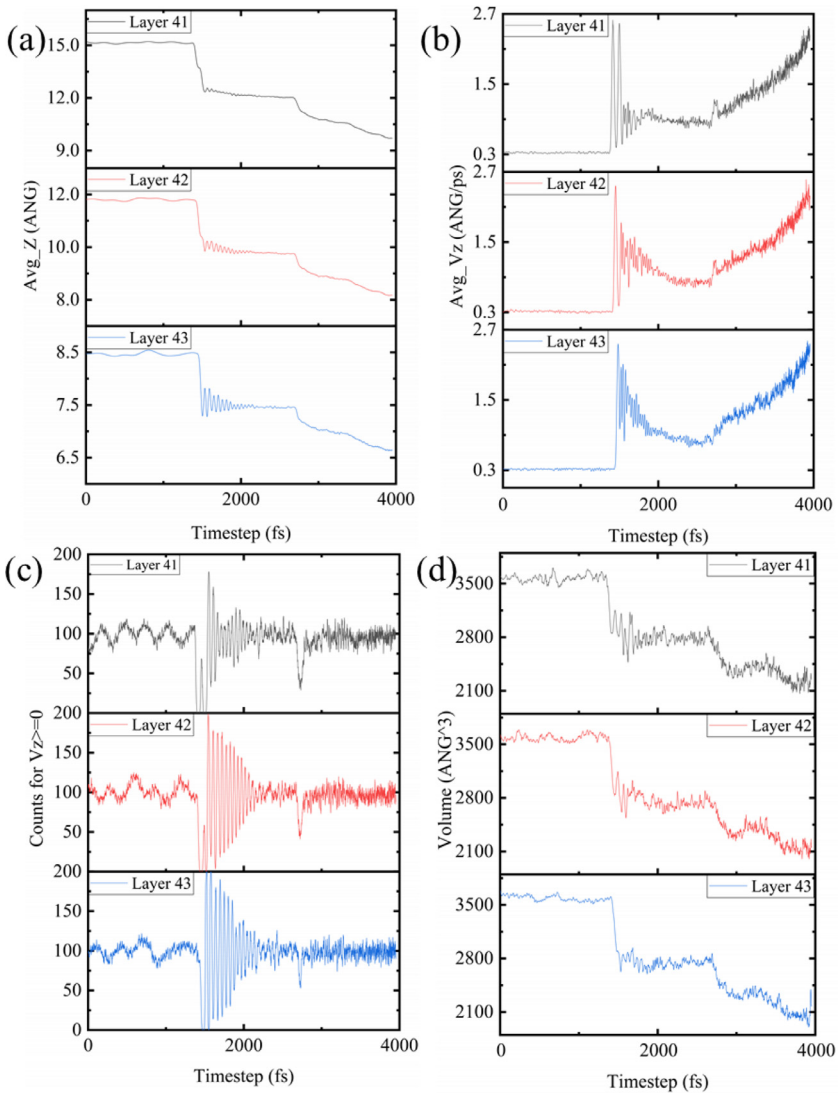

Fig. 6. Parameters during the simulation of laser shock on graphene layer 41, 42, 43 at 2 km/s piston velocity. (a) average position at Z axis. (b) average velocity at Z axis. (c) counts for Vz>=0. (d) volume around the layer.

ing direction of the piston, indicating the propagation of reflected shockwaves.

Apart from studying a scalar in Fig. 5b, we investigate a vector by counting the number of non-negative values of atomic velocity at the z axis for each layer in Fig. 5c. Counts for Vz>=0 drop because of the compression of the upper layer, indicating the propagation of incident shockwaves. While the counts rise because of the repulsion of the lower layer, indicating the propagation of reflected shockwaves. Results from Fig. 5b, c could further distinguish the compression and repulsion between layers and the influence of shockwaves. The variations of the curve are produced by the compression of the upper layer and repulsion of the lower layer. While the relatively long-term changes come from the incident shockwaves and the reflected shockwaves as we discussed above.

We also tracked the volume around the 5th, 15th, 25th and 35th layers to reveal the effect of incident shockwaves and reflected shockwaves. As shown in Fig. 5d, when incident shockwaves dominate, the compression happens from top layer to bottom layer. Layer of graphene absorbs the energy by losing surrounding space, transfers a small amount of it to a lower layer, and acts like a reservoir in flood times. When reflected shockwaves balance with incident shockwaves, the volume around the layer does not change much. Instead, it shows continual variations on volume, indicating frequent energy exchanges between layers. In this stage, graphene layers transfer the energy to the lower layer to avoid further losses of surrounding space. By moving back and forth, the graphene layer could steadily absorb and release the energy, which leads to almost equal compression to every interlayer in the model. At random sites of the graphite lattice, when critical distance between carbon atoms is reached under the as-mentioned compression, interlayer bonds and diamond phase will be formed correspondingly, which is also discussed in a previous study [40]. On the contrary, this mechanism will not happen in some high piston velocity models as shown in Fig. 3d, e. Because of the intensive collision with piston, their layered structure collapses at the beginning, making it difficult for energy to transfer to lower layers. Consequently, a large amount of carbon bonds breaks and amorphous carbon is formed.

To figure out the origin of reflected shockwaves, we traced the same parameters of layers 41st, 42nd and 43rd in Fig. 6. Note, the layers 44th and 45th were fixed as rigid boundary herein. Fig. 6a shows the stronger reflected shockwaves and weaker incident shockwaves bring abrupt compressions compared with Fig. 5a. Layer 41st achieves a smaller amplitude of variations of average position at Z axis compared with layer 42nd or layer 43rd. This emerges that as it propagates into the model, the reflected wave keeps losing energy to balance with the incident shockwaves. We also observed two peaks in layer 41st (Fig. 6b), while only one high peak was achieved for layer 42nd and layer 43rd. The first peak in the curve of layer 41st could be interpreted by the repulsion of layer 42nd. Thus, it could not be observed in the curves

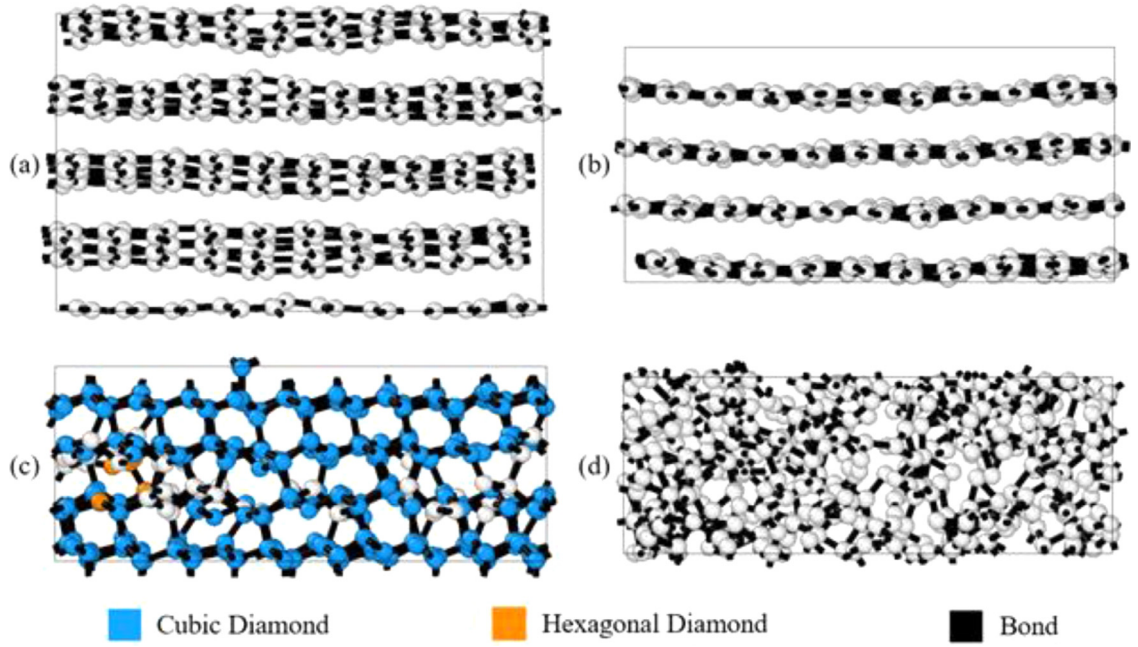

Fig. 7. Phase transfer of four trained structures under 2 km/s piston velocity at different times, (a) 0 ps, (b) 1.2 ps, (c) 2.4 ps, (d) 3.6 ps. (Unidentified atoms are colored in white.).

of layer 42nd and layer 43rd. The second peak of layer 41st is caused by the reflected wave from layer 43rd which can be identified in the curves of all 3 layers. The repulsion of layer 43rd is not identified because it overlaps with the reflected wave from layer 44th. We can also identify the first and second peaks in Fig. 6c. A trough at ~2700fs on the curves of all 3 layers, indicates the incident shockwaves dominate the bottom layers and balance with the reflected shockwaves immediately. This result matches the abrupt compression in Fig. 6a. 6d also confirms two abrupt compressions of Fig. 6a. The variations on the curves of Fig. 6b–d show the frequent energy exchanges between these three layers of 41st, 42nd and 43rd. Note that, in practical experiments, the graphite crystal boundary may not be as “rigid” as the boundary set in our MD model, but the energy exchanges surrounding the boundaries should be similar to cause reflected shockwaves. In addition, this effect will be more prominent in some synthesis processes with confined shockwaves.

In this section, we have discussed the origin, propagation, and reflection of shockwaves, which affect the formation of diamonds from graphite lattice. Next, we applied AIMD simulation to verify this phase transition in the shockwave process.

3.2. AIMD simulation of diamond formation

To confirm the formation of diamonds from graphite lattice, we trained four structures under 0 ps, 1.2 ps, 2.4 ps, 3.6 ps with a piston velocity of 2 km/s (Fig. 7). The mean interlayer spacings, the average spacing between adjacent layers from the second graphite layer to the fifth graphite layer for these structures, are 3.357 Å, 2.602 Å, 2.172 Å and 1.699 Å, respectively, indicating a continuous decrease during the shock compression (Fig. 7a-d). We found a slight decrease in temperature, from 2150 K to 1971 K, between structure 2 and 3, which could be explained by the formation of interlayer bonds, supporting the endothermic reaction of graphite to diamond transition during the simulation. In this process, the interlayer bond does not form immediately (Fig. 7a, b) even though the temperature rises to 2150 K due to the kinetic energy input from the piston. Instead, they form later in the further decreasing of interlayer spacing, whereas the cubic and hexagonal diamond structures could be identified. The result shows the graphite-to-diamond transition

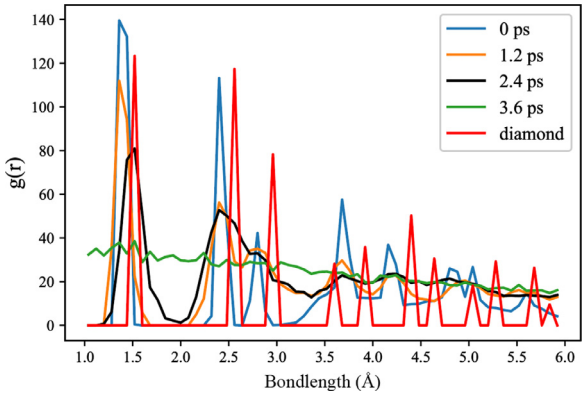

Fig. 8. Radial distribution function of diamond and four trained structures at different times.

is dominated by the decreasing interlayer spacing, rather than by the rise of temperature. Besides, the sp^3-sp^3 carbon bond could be identified especially in the top and bottom layers (Fig. 7c) in the AIMD simulation. Simulation results also show that the further compression would lead to the formation of amorphous carbon (Fig. 7d). Comparing Fig. 7 to Fig. 2, in the case of selecting the same simulation times steps, they present a similar phase transition process, e.g., the diamond structures were firstly identified at 2.4 ps in MD simulation and AIMD simulation. Although a small amount of diamond structures still exists in Fig. 2d while not in Fig. 7d, the difference could be explained by the different sizes of MD simulation and AIMD simulation. We can also observe that in MD simulation, these four layers are also distorted, consisting of a large amount of amorphous carbon atoms at 3.6 ps.

The radial distribution function (RDF) method is well accepted in analyzing graphite to diamond transition [41,42]. Here to verify the formation of diamond phase, the method is applied in the four trained structures above (Fig. 8). We can observe that the 1st or 2nd neighbor atoms at 0 ps and 1.2 ps (blue and orange lines) are closer to central atoms compared with that of diamond structure. At 2.4 ps, the leftmost black peak continually shifts to the right and even overlaps to that of the

diamond structure (red line), indicating diamond phase forms with the further decreases of the interlayer spacing, which confirms our results in Fig. 7. However, the peaks diminish at 3.6 ps as interlayer spacing further decreases, indicating the random distribution of atoms and the formation of amorphous carbon. It is also worth to note that, the two leftmost peaks exist at 2.4 ps, while other peaks diminish, and even further, all the peaks completely diminish at 3.6 ps, supporting the idea that the layered structure of graphite collapses and amorphous carbon atoms dominated at the structure of 3.6 ps in the AIMD simulation, which further supports the relationship of over-compression and amorphous carbon atoms as we discussed above.

4. Summary

In this paper, a computational model is developed to elucidate the graphite-to-diamond phase transition mechanism in the shockwave-based ND manufacturing process. The modeling results exhibit the tiered movement of the graphite layers and the frequent exchange of kinetic energy between the adjacent graphite layers, indicating the propagation of the incident shockwaves and the initiation of the reflected shockwaves. Therefore, the synergistic effect of incident and reflected shockwaves is investigated. The simulation results indicate that given the shockwave velocity up to roughly 12 km/s, the reflected shockwave contributes to the stabilization of the positions and energy of carbon atoms, leading to the formation of the interlayer bonds and the graphite-to-diamond phase transition. On the other hand, given the shockwave velocity higher than 16 km/s, the layered graphite structure is destroyed and the carbon atoms on the upper layers are amorphized, preventing the energy transferring to the bottom layers. Furthermore, the simulations demonstrate the origin of byproducts of amorphous carbon and carbon liquid during the shockwave-based ND manufacturing.

Declaration of Competing Interest

The authors declare that they have no known competing financial interests or personal relationships that could have appeared to influence the work reported in this paper.

Acknowledgements

Funding for this research was provided by National Science Foundation (NSF) under award numbers CMMI-1826439 and CMMI-1825739. This support is greatly acknowledged. The authors also thank the Agave Computer Cluster of ASU for providing the computational resources.

References

[1] M. Schwander, K. Partes, A review of diamond synthesis by CVD processes, Diam. Relat. Mater. 20 (9) (2011) 1287–1301.
[2] J. Field, The mechanical and strength properties of diamond, Rep. Prog. Phys. 75 (12) (2012) 126505.
[3] X. Yan, X. Li, X. Wang, H. Yan, Synthesis of nano-diamond/alumina composite by detonation method, Diam. Relat. Mater. 77 (2017) 79–83.
[4] V.N. Mochalin, O. Shenderova, D. Ho, Y. Gogotsi, The properties and applications of nanodiamonds, Nat. Nanotechnol. 7 (1) (2012) 11–23.
[5] R.J. Nemanich, J.A. Carlisle, A. Hirata, K. Haenen, CVD diamond—research, applications, and challenges, MRS Bull. 39 (6) (2014) 490–494.
[6] R. Sachan, S. Gupta, J. Narayan, Nonequilibrium structural evolution of Q-carbon and interfaces, ACS Appl. Mater. Interfaces 12 (1) (2019) 1330–1338.
[7] S.J. Turneaure, S.M. Sharma, T.J. Volz, J. Winey, Y.M. Gupta, Transformation of shock-compressed graphite to hexagonal diamond in nanoseconds, Sci. Adv. 3 (10) (2017) eaao3561.
[8] J. Dong, Z. Yao, M. Yao, R. Li, K. Hu, L. Zhu, Y. Wang, H. Sun, B. Sundqvist, K. Yang, Decompression-induced diamond formation from graphite sheared under pressure, Phys. Rev. Lett. 124 (6) (2020) 065701.
[9] S.C. Zhu, X.Z. Yan, J. Liu, A.R. Oganov, Q. Zhu, A revisited mechanism of the graphite-to-diamond transition at high temperature, Matter 3 (3) (2020) 864–878.
[10] Z. Liang, X. Jia, H. Ma, C. Zang, P. Zhu, Q. Guan, H. Kanda, Synthesis of HPHT diamond containing high concentrations of nitrogen impurities using NaN3 as dopant in metal-carbon system, Diam. Relat. Mater. 14 (11–12) (2005) 1932–1935.
[11] D.D. Damm, A. Contin, F.C. Barbieri, V.J. Trava-Airoldi, D.M. Barquete, E.J. Corat, Interlayers applied to CVD diamond deposition on steel substrate: a review, Coatings 7 (9) (2017) 141.
[12] M. Lobaev, A. Gorbachev, S. Bogdanov, A. Vikharev, D. Radishev, V. Isaev, V. Chernov, M. Drozdov, Influence of CVD diamond growth conditions on nitrogen incorporation, Diam. Relat. Mater. 72 (2017) 1–6.
[13] Z. Yiming, F. Larsson, K. Larsson, Effect of CVD diamond growth by doping with nitrogen, Theor. Chem. Acc. 133 (2) (2014) 1–12.
[14] F. Huang, P. Liang, X. Yang, H. Cai, J. Wu, N. Xu, Z. Ying, J. Sun, Confinement effects of shock waves on laser-induced plasma from a graphite target, Phys. Plasmas 22 (6) (2015) 063509.
[15] D. Kraus, A. Ravasio, M. Gauthier, D. Gericke, J. Vorberger, S. Frydrych, J. Helfrich, L. Fletcher, G. Schaumann, B. Nagler, Nanosecond formation of diamond and lonsdaleite by shock compression of graphite, Nat. Commun. 7 (1) (2016) 1–6.
[16] A. Kurdyumov, V. Britun, V. Yarosh, A. Danilenko, V. Zelyavskii, The influence of the shock compression conditions on the graphite transformations into lonsdaleite and diamond, J. Superhard Mater. 34 (1) (2012) 19–27.
[17] C.J. Mundy, A. Curioni, N. Goldman, I.-.F. Will Kuo, E.J. Reed, L.E. Fried, M. Ianuzzi, Ultrafast transformation of graphite to diamond: an ab initio study of graphite under shock compression, J. Chem. Phys. 128 (18) (2008) 184701.
[18] D. Veysset, T. Pezeril, S. Kooi, A. Bulou, K.A. Nelson, Laser-induced versus shock wave induced transformation of highly ordered pyrolytic graphite, Appl. Phys. Lett. 106 (16) (2015) 161902.
[19] J. Winey, Y. Gupta, Shock-compressed graphite to diamond transformation on nanosecond time scales, Phys. Rev. B 87 (17) (2013) 174104.
[20] V.D. Blank, V.D. Churkin, B.A. Kulnitskiy, I.A. Perezhogin, A.N. Kirichenko, V.N. Denisov, S.V. Erohin, P.B. Sorokin, M.Y. Popov, Phase diagram of carbon and the factors limiting the quantity and size of natural diamonds, Nanotechnology 29 (11) (2018) 115603.
[21] M.Y. Popov, V.D. Churkin, B.A. Kulnitskiy, A.N. Kirichenko, K.M. Bulatov, A.A. Bykov, P.V. Zinin, V. Blank, Transformation of diamond to fullerene-type onions at pressure 70 GPa and temperature 2400 K, Nanotechnology 31 (31) (2020) 315602.
[22] X. Zhang, H. Sun, B. Mao, R. Dai, H. Zhuang, Y. Liao, Q. Nian, Nanosecond laser shock detonation of nanodiamonds: from laser-matter interaction to graphite-to-diamond phase transition, Int. J. Extreme Manuf. 4 (1) (2021) 015401.
[23] Q. Nian, Y. Wang, Y. Yang, J. Li, M.Y. Zhang, J. Shao, L. Tang, G.J. Cheng, Direct laser writing of nanodiamond films from graphite under ambient conditions, Sci. Rep. 4 (1) (2014) 1–8.
[24] M. Mandal, F. Haso, T. Liu, Y. Fei, K. Landskron, Size tunable synthesis of solution processable diamond nanocrystals, Chem. Commun. 50 (77) (2014) 11307–11310.
[25] A.K. Khachatryan, S. Aloyan, P. May, R. Sargsyan, V. Khachatryan, V. Baghdasaryan, Graphite-to-diamond transformation induced by ultrasound cavitation, Diam. Relat. Mater. 17 (6) (2008) 931–936.
[26] V. Aksenenkov, V. Blank, N. Borovikov, V. Danilov, K. Kozorezov, Production of diamond single crystals in graphite under plastic deformation, Phys. Dokl. (1994) 700–703.
[27] F. Bundy, Direct conversion of graphite to diamond in static pressure apparatus, J. Chem. Phys. 38 (3) (1963) 631–643.
[28] F. Bundy, W. Bassett, M. Weathers, R. Hemley, H. Mao, A. Goncharov, The pressure-temperature phase and transformation diagram for carbon; updated through 1994, Carbon 34 (2) (1996) 141–153 N Y.
[29] T.C. O'Connor, J. Andzelm, M.O. Robbins, AIREBO-M: a reactive model for hydrocarbons at extreme pressures, J. Chem. Phys. 142 (2) (2015) 024903.
[30] S. Plimpton, Fast parallel algorithms for short-range molecular dynamics, J. Comput. Phys. 117 (1) (1995) 1–19.
[31] A. Stukowski, Visualization and analysis of atomistic simulation data with OVITO–the open visualization tool, Model. Simul. Mater. Sci. Eng. 18 (1) (2009) 015012.
[32] J.P. Perdew, K. Burke, M. Ernzerhof, Generalized gradient approximation made simple, Phys. Rev. Lett. 77 (18) (1996) 3865.
[33] G. Kresse, J. Furthmüller, Efficiency of ab-initio total energy calculations for metals and semiconductors using a plane-wave basis set, Comput. Mater. Sci. 6 (1) (1996) 15–50.
[34] G. Kresse, J. Furthmüller, Efficient iterative schemes for ab initio total-energy calculations using a plane-wave basis set, Phys. Rev. B 54 (16) (1996) 11169.
[35] K. Katagiri, N. Ozaki, Y. Umeda, T. Irifune, N. Kamimura, K. Miyanishi, T. Sano, T. Sekine, R. Kodama, Shock response of full density nanopolycrystalline diamond, Phys. Rev. Lett. 125 (18) (2020) 185701.
[36] K.i. Kondo, T.J. Ahrens, Shock compression of diamond crystal, Geophys. Res. Lett. 10 (4) (1983) 281–284.
[37] A. Schropp, R. Hoppe, V. Meier, J. Patommel, F. Seiboth, Y. Ping, D.G. Hicks, M.A. Beckwith, G.W. Collins, A. Higginbotham, Imaging shock waves in diamond with both high temporal and spatial resolution at an XFEL, Sci. Rep. 5 (1) (2015) 1–8.
[38] S. Signetti, K. Kang, N.M. Pugno, S. Ryu, Atomistic modelling of the hypervelocity dynamics of shock-compressed graphite and impacted graphene armours, Comput. Mater. Sci. 170 (2019) 109152.
[39] E. Maras, O. Trushin, A. Stukowski, T. Ala-Nissila, H. Jonsson, Global transition path search for dislocation formation in Ge on Si (001), Comput. Phys. Commun. 205 (2016) 13–21.
[40] D. Ovsyannikov, V. Zhukov, T. Gordeeva, L. Antipina, P. Sorokin, B. Kulnitskiy, M. Popov, V. Blank, Intermediate carbon phase. New experimental data and atomic model, Diam. Relat. Mater. 123 (2022) 108825.
[41] L. He, T.D. Sewell, D.L. Thompson, Molecular dynamics simulations of shock waves in oriented nitromethane single crystals, J. Chem. Phys. 134 (12) (2011) 124506.
[42] J. Zhao, C. Zhang, F. Liu, G.J. Cheng, Understanding femtosecond laser internal scribing of diamond by atomic simulation: phase transition, structure and property, Carbon 175 (2021) 352–363 N Y.